

La₂O₃Fe₂Se₂, a Mott insulator on the brink of orbital-selective metalization

Gianluca Giovannetti,^{1,2} Luca de' Medici,³ Markus Aichhorn,⁴ and Massimo Capone^{2,1}

¹*CNR-IOM-Democritos National Simulation Centre,*

UoS Trieste-SISSA, Via Bonomea 265, I-34136, Trieste, Italy

²*International School for Advanced Studies (SISSA), Via Bonomea 265, I-34136, Trieste, Italy*

³*European Synchrotron Radiation Facility, BP 220, F-38043 Grenoble Cedex 9, France*

⁴*Institute of Theoretical and Computational Physics, TU Graz, Petersgasse 16, Graz, Austria*

We show that the insulating character of the iron-selenide La₂O₃Fe₂Se₂ can be explained in terms of Mott localization in sharp contrast with the metallic behavior of FeSe and other parent compounds of iron superconductors. We demonstrate that the key ingredient that makes La₂O₃Fe₂Se₂ a Mott insulator, rather than a correlated metal dominated by the Hund's coupling is the enhanced crystal-field splitting, accompanied by a smaller orbital-resolved kinetic energy. The strong deviation from orbital degeneracy introduced by the crystal-field splitting also pushes this materials close to an orbital-selective Mott transition. We predict that either doping or uniaxial external pressure can drive the material into an orbital-selective Mott state, where only one or few orbitals are metallized while the others remain insulating.

PACS numbers: 71.30.+h, 71.10.Fd, 71.27.+a

I. INTRODUCTION

The link between high-temperature superconductivity and strong electron-electron correlations has been forged and strengthened by decades of investigation in the copper-based superconductors (cuprates). In this light, the debate about the strength and the role of electron correlations in iron-based superconductors (FeSC) maintains a crucial importance. The overall phenomenology of these materials does not provide a self-evident answer. In these materials superconductivity appears doping a metallic spin-density-wave parent compound, rather than the Mott insulator of the cuprates, and, while the metallic state is highly incoherent, the standard fingerprints of strong correlations, like the Hubbard bands, are not universally observed.

Furthermore non-perturbative studies of the effect of the interactions, mainly based on Dynamical Mean-Field Theory (DMFT) and related methods, have highlighted a novel behavior, in which the Hund's coupling J_h to play a major role in determining the degree of correlations^{1,2}. The electrons in the d-orbitals (the parent compounds have a nominal filling of six electrons for each iron atom) are strongly correlated, as measured by the bad-metallic behavior with small coherence scales shown in many experiments, but the Hubbard repulsion U is substantially smaller than the critical value for the Mott transition^{3,4}. This regime is often labeled as a "Hund's metal" and displays characteristic properties^{5,6} including a remarkable tendency to "orbital selectivity", i.e., to a neat differentiation in the degree of correlation of the different orbitals, leading to the simultaneous presence of weakly and strongly correlated electrons^{4,7-10}. In Ref.¹⁰ it has been shown that the Hund's coupling decouples the orbitals quenching the inter-orbital fluctuations and that this leads to a picture of five doped single-band Mott insulators. Consequently the degree of correlation is controlled by the distance of each individual orbital from the

half-filled d^5 configuration. The relevance of the d^5 Mott phase in the phase diagram of models for iron superconductors has been observed also in 11.

While no iron-based material can be doped with one hole per iron site, isostructural materials where iron is replaced with manganese are characterized by the d^5 half-filled configuration and they are indeed antiferromagnetic Mott insulators.¹²⁻¹⁴ However, the evidence for strong-correlation physics in the FeSC does can not rely on the presence of actual Mott states directly connected with the superconducting compounds. Indeed no Mott insulator exists in the 122 family (BaFe₂As₂ or isoelectronic compounds doped either with holes and electrons), the 1111 family which originates doping LaFeAsO, the 11 selenides FeSe and FeTe, and LiFeAs. While this experimental fact is indeed completely compatible with the scenario based on the Hund's coupling, it may cast doubts on the whole relevance of correlations.

A close relative of FeSC with insulating behavior is La₂O₃Fe₂Se₂. This system is based on a square lattice of Fe ions with nominal valence 2+ as in all of iron pnictides and chalcogenides. However, the resistivity as a function of temperature shows clearly an insulating behavior with an activation energy gap of about 0.19 eV.¹⁵ On the basis of this experimental evidence combined with Density-Functional Theory (DFT) supplemented by mean-field treatment of the Hubbard U (DFT+ U) in the ordered magnetic phase it has been argued that La₂O₃Fe₂Se₂ is in a Mott state with low-temperature antiferromagnetic ordering.¹⁵ This evidence raises the natural question about the reason why the Hund's metallic behavior of undoped FeSC is replaced with a Mott state in this compound. A simple bandwidth reduction is a very unlikely answer, since one of the defining properties of the Hund's metal regime is that the critical value for a Mott transition is pushed to very large values, significantly far from the experimental estimates.¹⁶ This calls for the identification of specific aspects of the bandstruc-

ture which make the present material insulating.

In this work we investigate the differences of the electronic structure of $\text{La}_2\text{O}_3\text{Fe}_2\text{Se}_2$ with respect to parent compounds of the FeSC using the reference case of FeSe. We identify in a strong lifting of the orbital degeneracy the main difference of the material under consideration with respect to most parent compounds of iron-based superconductors. This leads to a marked tendency towards orbital-selective Mott transition and opens the way to a complete Mott localization when combined with the reduced kinetic energy of $\text{La}_2\text{O}_3\text{Fe}_2\text{Se}_2$ with respect to FeSe.

The paper is organized as follows. In Sec. II we present the electronic structure which emerges from Density-Functional Theory calculations, while In Sec. III we consider the inclusion of electron-electron interactions. The section is organized in two subsections dedicated respectively to the results obtained within the slave-boson mean-field scheme and the more accurate Dynamical Mean-Field Theory. Sec. IV contains our conclusions.

II. DENSITY-FUNCTIONAL THEORY BANDSTRUCTURE

We start our investigation determining the bandstructure of $\text{La}_2\text{O}_3\text{Fe}_2\text{Se}_2$ by means of DFT in the framework of the generalized gradient approximation (using the Perdew-Burke-Ernzerhof (PBE) functional¹⁷) for the tetragonal unit cell of $\text{La}_2\text{O}_3\text{Fe}_2\text{Se}_2$ ¹⁵ using Quantum Espresso¹⁸ and Wien2K¹⁹. In Fig. 1 we show the density of states projected on the different atoms.

PBE calculations clearly lead to a metallic solution with a sizable spectral weight at the Fermi level. This low-energy contribution to the spectral density is dominated by the bands arising from Fe 3d electrons, which are very weakly entangled with oxygen and lanthanum bands lying in energy windows far from the Fermi level. The 3d bands have an overall width of 3.2 eV, considerably narrower than the 4.6 eV of the same bands in FeSe^{2,4}.

In order to include the on-site Coulomb interaction parameterized by the Hubbard U and the Hund's coupling J_h we compute maximally localized Wannier orbitals²⁰ for the pure 3d Fe orbitals built from the iron bands in the energy range between -2 and 1.2 eV. The properties of these orbitals will also provide us with important information that will help us to rationalize the behavior of this materials.

The on-site energies of the Wannier orbitals reflect indeed an important difference between the material under consideration and the parent compounds of the iron-based superconductors. In $\text{La}_2\text{O}_3\text{Fe}_2\text{Se}_2$, the Fe ions are surrounded by two nearby oxygen anions and four distant selenium anions. The additional oxygen ions result in a lower symmetry in $\text{La}_2\text{O}_3\text{Fe}_2\text{Se}_2$ as compared to FeSe and other FeSC. This means that the local problem is no longer diagonal in the stan-

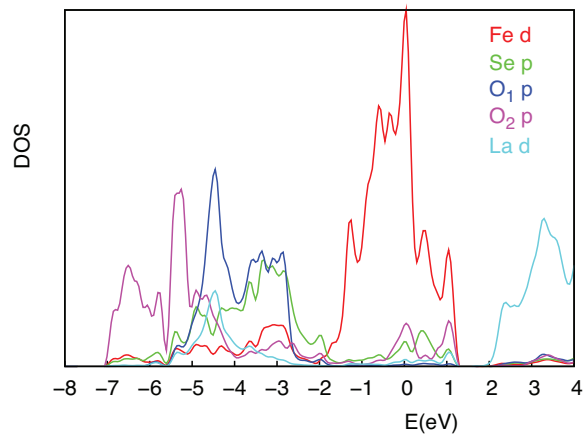


FIG. 1. (Color online) Density of states of $\text{La}_2\text{O}_3\text{Fe}_2\text{Se}_2$ calculated within PBE and projected on the different atomic species. The zero energy is set at the Fermi level.

dard cubic basis defined by the e_g and t_{2g} orbitals. We can obviously diagonalize the local Hamiltonian for $\text{La}_2\text{O}_3\text{Fe}_2\text{Se}_2$ by means of a unitary transformation. The resulting orbitals, which are linear combinations of the $(3z^2 - r^2, xz, yz, x^2 - y^2, xy)$ orbitals²¹ that we label as (1, 2, 3, 4, 5) have in our calculations on-site energy of $(-0.660, -0.627, -0.397, 0.183, 0.543)$ eV, respectively. This leads to a total crystal-field splitting of 1.1 eV, much larger than the value for FeSe, which we estimate in 0.48 eV within analogous PBE calculations.

Comparing the orbital-resolved density of states for $\text{La}_2\text{O}_3\text{Fe}_2\text{Se}_2$ and FeSe (see Fig. 2) we can visualize the different crystal-field splitting and emphasize another related effect: in FeSe the different orbitals have a similar width and lie more or less in the same energy range. In contrast $\text{La}_2\text{O}_3\text{Fe}_2\text{Se}_2$ features a set of narrow orbitals significantly shifted in energy relative to each other. That means that the effective band-width reduction for each individual orbital is even larger than the factor estimated from the total band width. Interestingly, even in FeSe and other standard FeSC it has been shown²² that, arbitrarily neglecting interorbital hybridizations turns the broad orbitals into more localized objects, similar to what we find for $\text{La}_2\text{O}_3\text{Fe}_2\text{Se}_2$. Therefore we can link the peculiar orbital-resolved density of states of the latter material with the crystal-field splitting that reduces the effect of the interorbital hybridization.

In the following of the paper we investigate how the difference in the single-particle spectra reflects on the effects of electron-electron correlations, keeping in mind the role of the Hund's coupling that we anticipated above. The results picture can be quite rich because of the non-trivial interplay between the ‘‘Hund's physics’’ and the two main differences we highlighted, a reduced kinetic energy and an increased crystal-field splitting. In particular, while a reduced kinetic energy simply leads to effectively larger Coulomb terms, the crystal-field splitting competes with the Hund's coupling, as the latter tries to spread the elec-

trons among the different orbitals to maximize the total spin, while a large crystal-field splitting obviously favors an unbalanced population with large occupation of the low-lying orbitals.

III. EFFECT OF ELECTRON-ELECTRON CORRELATIONS

To understand the role of electron-electron interactions in turning $\text{La}_2\text{O}_3\text{Fe}_2\text{Se}_2$ insulating we consider two different approaches to treat the short-range interactions. We start from a Slave-Spins mean-field (SSMF) theory²³, which allows for a computationally inexpensive and fast survey of the phase diagram and it is expected to capture the main physics as long as the system remains in a Fermi-liquid state¹⁰. Then we move to the more accurate DFT+Dynamical Mean-Field Theory (DMFT)²⁴ method, which treats exactly the local quantum dynamics mapping the lattice model onto an impurity embedded in a self-consistent bath. As impurity solver we employ mainly Exact Diagonalization (ED).^{25,26} We verified for selected parameter the excellent agreement of ED with the continuous-time Quantum Monte Carlo solution of the impurity model implemented in the TRIQS toolkit^{27–29}.

For the interacting part of the Hamiltonian we use a Kanamori form parameterized by U and J_h according to

$$\begin{aligned}
H_{int} = & U \sum_{i,m} n_{im\sigma} n_{im\sigma'} + U' \sum_{i,m,m'} n_{im\sigma} n_{im'\sigma'} + \\
& + U'' \sum_{i,m,m'} n_{im\sigma} n_{im'\sigma} + \\
& - J_h \sum_{i,m,m'} [d_{im\uparrow}^+ d_{im'\downarrow}^+ d_{im\downarrow} d_{im'\uparrow} + \\
& + d_{im\uparrow}^+ d_{im'\downarrow}^+ d_{im'\uparrow} d_{im\downarrow}] \quad (1)
\end{aligned}$$

where $d_{i,m\sigma}$ is the destruction operator of an electron of spin σ at site i in orbital m , and $n_{im\sigma} = d_{im\sigma}^+ d_{im\sigma}$, U and $U' = U - 2J_h$, $U'' = U - 3J_h$ are intra- and inter-orbital repulsions and J_h is the Hund's coupling. In the absence of estimates of U and J_h for this material, we use the constrained random-phase-approximation (cRPA) for FeSe ($U = 4.2\text{eV}$ and $J_h = 0.504\text{eV}$) which are not expected to differ in a critical way.²² Note that these interaction values are given in Hubbard-Kanamori notation. The use of the same parameters also allows us to highlight the role of the material-specific properties (kinetic energy and crystal-field splitting) in determining the low-energy properties of the system. In all the calculations we consider paramagnetic solution that preserve also the orbital symmetry.

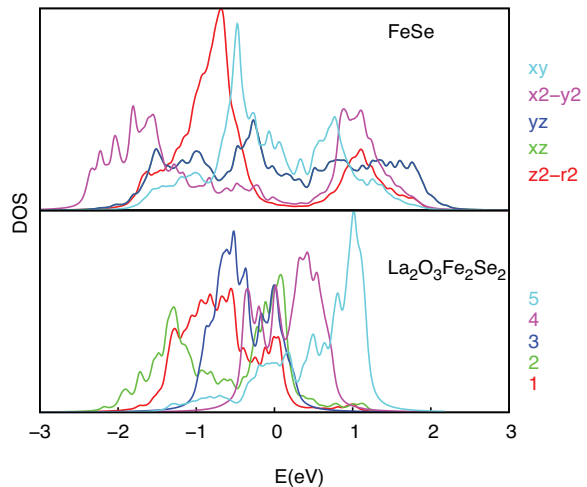


FIG. 2. (Color online) Orbital-resolved density of states for $\text{La}_2\text{O}_3\text{Fe}_2\text{Se}_2$ (bottom panel) and FeSe (top panel). The zero energy is set at the Fermi level.

A. Slave-spin Mean-Field Approximation

In Fig. 3 we show the DFT+SSMF orbital resolved densities n_m and quasiparticle weights Z_m as functions of Coulomb parameter U at fixed ratio $J_h/U = 0.2$. Within this approximation spin-flip and pair-hopping terms (last two lines of Eq. (1)) are not included. Z_m is the measure of the metallic character of each orbital. A vanishing of Z_m for a given orbital implies that the carriers with that character are reaching a Mott localization. A Mott insulating state is reached when all the Z_m 's vanish, while a situation with coexisting finite and zero Z_n 's would correspond to an orbital-selective Mott transition (OSMT).

For small interactions, up to $U \simeq 1.5\text{eV}$, the orbital densities range from 0.22 to 0.8 and the Z_m are close to one. Increasing U , the Z_m decrease and depart from each other while the orbital populations deviate substantially from the non-interacting values. More precisely, the orbitals labeled as 4, 3 and 5 move, one after the other, towards a half-filled configuration ($n_m = 0.5$) and they become insulating ($Z_m = 0$) at different interaction strengths. In other words, the system shows a series of OSMT's in which the different orbitals become localized independently on the behavior of the others. The two remaining orbitals (1 and 2) instead remain metallic for a larger range of interactions and they simultaneously become insulating for $U_c = 3.6\text{eV}$, smaller than the estimated value for FeSe. At this critical interaction also orbital 2 becomes half-filled, while orbital 1 is completely filled. The "order" in which the different orbitals undergo a Mott transition is a consequence of the individual bandwidth, which is smaller for orbitals 4 and 3 and of the initial orbital population.

The series of transitions that we described is in stark contrast with the results for FeSe⁴ and for the other parent compounds^{9,10}, where no OSMT occurs despite a

marked differentiation between the Z_m of the different orbitals. In this case a full Mott transition in which all the orbitals become simultaneously localized takes place for values of the interactions which are much larger than reasonable estimates for this material. In particular, for the cRPA values (for FeSe) introduced above, $\text{La}_2\text{O}_3\text{Fe}_2\text{Se}_2$ is a Mott insulator, while FeSe is a Hund's metal with small and orbital-differentiated quasiparticle weights.

It is useful to notice that, increasing the value of J_h the critical coupling for an OSMT is reduced, while the critical U for a full Mott transition increases³⁰. This result, together with the whole picture we have drawn, is in perfect agreement with model calculations in which orbitals with the same bandwidth have been shifted leading to an OSMT^{7,30}.

Interestingly, while the full Mott localization requires a commensurate filling, the OSMT that we observed survive also doping the d^6 Mott insulator. In the inset of Fig. 3 we show the evolution of the quasiparticle weight as a function of U for a $d^{5.5}$ configuration, where we doped one hole every two iron sites. Comparing with the d^6 case, we see that orbitals 3, 4 and 5 still undergo the series of OSMT's we described above, and in particular the three orbitals are insulating for the U values representative of $\text{La}_2\text{O}_3\text{Fe}_2\text{Se}_2$, while orbitals 1 and 2 become metallic after doping. This can be explained in terms of a schematic general picture of OSMT³¹. For sizable J/U the global half-filled configuration is in general a Mott insulator at quite smaller U than for the d^6 case. In this d^5 Mott insulating phase each orbital opens an independent gap, thus being half-filled when the chemical potential falls within its gap. The gaps can have different widths and position depending on the crystal-field splitting and the bandwidth of their orbital. Doping of a Mott insulator occurs essentially when the chemical potential moves out of the gap, and thus in this situation this happens for each orbital at a separate value of the chemical potential. The selective doping of one or more orbitals leads therefore to an OSMT. Our results show that the bandstructure of $\text{La}_2\text{O}_3\text{Fe}_2\text{Se}_2$ is such that when reaching a total filling of 6 electrons only two orbitals (1,2) have actually been doped compared to the half-filled case while the rest remain half-filled, have an open gap, and are thus insulating. This does not depend on the filling being exactly 6 or slightly above or below, thus doping the d^6 configuration tunes indeed the Mott transition for orbitals 1 and 2 but does not alter the selective insulating behavior for orbitals 3,4,5.

Our results strongly indicate that the main anomaly of $\text{La}_2\text{O}_3\text{Fe}_2\text{Se}_2$ with respect to the parent compounds of FeSC is the strong enhancement of the crystal-field splitting with respect to iron-based superconductors, which conjures with the Hund's coupling to decouple the different orbitals, leading to an orbital selective localization rather than to a global Mott transition for the six electrons. The overall reduction of the kinetic energy with respect to FeSe plays a more quantitative role, reducing the actual critical value of U .

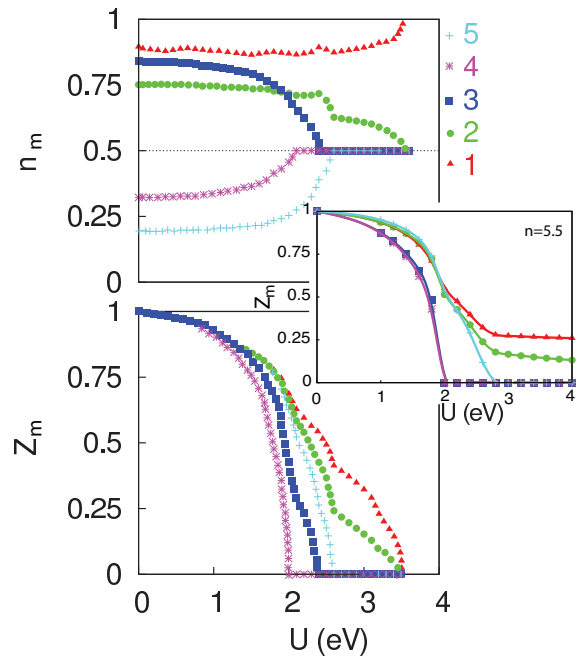


FIG. 3. (Color online) Orbitaly resolved density (n_m) and quasiparticle weights (Z_m) calculated within DFT + SSMF for $\text{La}_2\text{O}_3\text{Fe}_2\text{Se}_2$ at ratio $J_h/U = 0.20$. The inset shows Z_m for a filling of $d^{5.5}$ electrons per iron (one hole every two iron sites).

B. Dynamical Mean-Field Theory

Our DFT+SSMF treatment is however limited to metallic solutions and it can not help us to characterize the Mott insulating solution for $U > U_c$. A full description of both low- and high-energy features can instead be obtained by means of DFT+DMFT. As mentioned above, we mainly use an ED solution for the impurity model, which also allows us to include pair-hopping and spin-flip terms, as opposed to DFT+SSMF.

We consider $N_s = 15$ orbitals in total, with 5 impurity orbitals and 2 bath degrees of freedom connected to each impurity orbital. The storage requirements for the matrix hamiltonian and Lanczos vector, since the Hilbert space has dimension 41 409 225, are solved by splitting them over parallel processors. The impurity solver is diagonalized by a parallel Arnoldi algorithm³² using the symmetry with respect to the inversion of up and down particles.

In Fig. 3 we show the dynamical information obtained for the cRPA values $U = 4.2$ eV and $J_h = 0.504$ eV. We present orbital-resolved Green's functions on the imaginary-frequency axis (a)), which is the most direct product of the calculation, and the real-frequency spectral function (b)), which provides a more obvious physical content. The imaginary part of the Matsubara Green's functions smoothly extrapolate to zero in the limit of small frequency. This clearly confirms that the material is insulating also within the more accurate DFT+DMFT

method. The imaginary part of the self-energy diverges only for orbital 5, for which the chemical potential happens to lie in the middle of the gap (See also the spectral function in panel b)). For the other orbitals the chemical potential lies far from the center of the gap and, consequently, the imaginary part of the self-energy does not diverge. Finally, a comparison of the orbital-projected spectral density with the DFT results of Fig. 1 allows us to visualize the formation of high-energy spectral weight due to strong correlations and to estimate the Mott gap $\Delta_{Mott} \simeq 1eV$. The Mott insulating state of $La_2O_3Fe_2Se_2$ is characterized by a high-spin configuration with $S = 2$ as a consequence of the Hund's coupling. The orbital populations are in agreement with the DFT+SSMF results, confirming the picture of four half-filled orbitals and one full orbital. Therefore the whole scenario obtained within DFT+SSMF survives when we move to the full DMFT treatment of correlations, suggesting that also the sequence of OSMT transition preceding the full Mott localization is a real feature of the present material. The disagreement between the theoretical value of the gap and experiments may be attributed to an overestimate of U and J_h , or even in their ratio. However, as mentioned above, the choice to use the same values of FeSe allowed us to highlight the difference between $La_2O_3Fe_2Se_2$ and the parent compounds of standard FeSC.

All the calculations we presented are limited to a paramagnetic solution without broken symmetry in any channel, demonstrating the intrinsic Mott character of the insulating state. However, at low temperature this state may be unstable towards different ordering as magnetic and orbitals ones^{33,34} as it is indeed suggested by DFT+U calculations¹⁵.

To confirm the reliability of our results, we compared with a different DFT+DMFT implementation based on the TRIQS package.²⁷⁻²⁹ In these calculation we use projective Wannier function techniques, as well as continuous-time quantum Monte Carlo as impurity solver. In addition, we considered also the Se p states for the construction of the Wannier functions, in order to check the stability of the insulating state. For the interactions we use also cRPA values for FeSe, and a Slater expansion of the interaction hamiltonian².

The results confirms the precedent picture. The system is in a Mott state, with four orbitals close to half-filling, and one completely filled. The insulating state appears therefore extremely solid, as it does not depend on the details of the computational scheme that is applied.

IV. CONCLUSIONS

In conclusion, we use different approaches combining DFT with strong correlation physics to study the electronic properties of the new synthesized compound $La_2O_3Fe_2Se_2$, an insulating material that shares the same electron count with the metallic parent compounds of

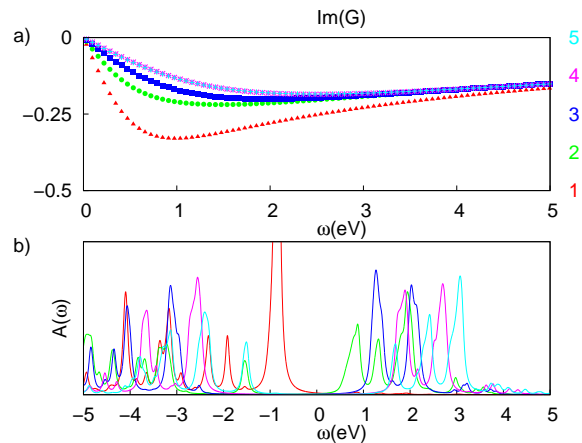


FIG. 4. (Color online) a) Orbital-resolved imaginary part of local Green's function (G) as a function of the Matsubara imaginary frequency, b) spectral density (A) as a function of the real frequency computed within DFT + DMFT for $La_2O_3Fe_2Se_2$.

iron superconductors. Our calculations clearly demonstrate that the material is a Mott insulator. A detailed understanding of the electronic structure of $La_2O_3Fe_2Se_2$ compared to the one of FeSe highlights the difference of this class of compounds with ordinary Fe-based superconducting materials. Using the same interaction values for the two materials, we demonstrate that the insulating behavior of $La_2O_3Fe_2Se_2$ is not simply due to a larger interaction strength, but it is related to a more fundamental difference in the electronic structure.

We identify the main reason for the insulating behavior in the enhancement of the crystal-field splitting due to the position of the oxygen atoms. The larger crystal-field leads to a reduced overlap between the density of states with different orbital character, which triggers a series of successive Mott transitions in which the different orbitals become insulating one after the other as the interaction grows. The insulator is indeed characterized by four singly occupied orbitals and a fully occupied one. This condition is quite different from iron-based superconductors, in which a marked orbital differentiation does not however lead to individual Mott insulating behavior.

As a consequence, we predict that $La_2O_3Fe_2Se_2$ should give rise to a series of OSMT under pressure and we expect that a similar behavior should take place as a function of doping. A slightly doped material is expected to show the coexistence between localized orbitals and delocalized orbitals hosting the extra charges.

Note Added. During completion of this work, we became aware of a related work by B. Freelon et Al., which is complementary to ours and gives comparable results.

ACKNOWLEDGMENTS

GG and MC are financed by European Research Council under FP7/ERC Starting Independent Research Grant “SUPERBAD” (Grant Agreement n. 240524).

MA is supported from the Austrian Science Fund (FWF) through projects F04103, P26220, and Y746. Calculations have been performed at CINECA within the HPCproject 2014 CONDMAG (IsB04) and the TU Graz dcluster.

-
- ¹ K. Haule and G. Kotliar, *New Journal of Physics* **11**, 025021 (2009).
- ² M. Aichhorn, S. Biermann, T. Miyake, A. Georges, and M. Imada, *Physical Review B* **82**, 064504 (2010).
- ³ L. de’ Medici, *Phys. Rev. B* **83**, 205112 (2011).
- ⁴ N. Lanatà, H. U. R. Strand, G. Giovannetti, B. Hellsing, L. de’ Medici, and M. Capone, *Phys. Rev. B* **87**, 045122 (2013).
- ⁵ Z. P. Yin, K. Haule, and G. Kotliar, *Phys. Rev. B* **86**, 195141 (2012).
- ⁶ P. Hansmann, R. Arita, A. Toschi, S. Sakai, G. Sangiovanni, and K. Held, *Phys. Rev. Lett.* **104**, 197002 (2010).
- ⁷ L. de’ Medici, S. Hassan, and M. Capone, *J. Supercond. Nov. Mag.* **22**, 535 (2009).
- ⁸ S.-P. Kou, T. Li, and Z.-Y. Weng, *EPL (Europhysics Letters)* **88**, 17010 (2009); A. Hackl and M. Vojta, *New Journal of Physics* **11**, 055064 (2009); W.-G. Yin, C.-C. Lee, and W. Ku, *Phys. Rev. Lett.* **105**, 107004 (2010); W. Lv, F. Krüger, and P. Phillips, *Phys. Rev. B* **82**, 045125 (2010); **10**; R. Yu and Q. Si, *Phys. Rev. B* **84**, 235115 (2011); E. Bascones, B. Valenzuela, and M. Calderón, *Phys. Rev. B* **86**, 174508 (2012); Y.-Z. Zhang, H. Lee, H.-Q. Lin, C.-Q. Wu, H. Jeschke, and R. Valentí, *Phys. Rev. B* **85**, 035123 (2012).
- ⁹ R. Yu and Q. Si, *Phys. Rev. B* **86**, 085104 (2012).
- ¹⁰ L. de’ Medici, G. Giovannetti, and M. Capone, *Phys. Rev. Lett.* **112**, 177001 (2014).
- ¹¹ H. Ishida and A. Liebsch, *Phys. Rev. B* **81**, 054513 (2010); H. Ikeda, R. Arita, and J. Kuneš, *Phys. Rev. B* **82**, 024508 (2010); T. Misawa, K. Nakamura, and M. Imada, *Phys. Rev. Lett.* **108**, 177007 (2012).
- ¹² Y. Singh, M. A. Green, Q. Huang, A. Kreyssig, R. J. McQueeney, D. C. Johnston, and A. I. Goldman, *Phys. Rev. B* **80**, 100403 (2009).
- ¹³ H. Yanagi, T. Watanabe, K. Kodama, S. Iikubo, S. Shamoto, T. Kamiya, M. Hirano, and H. Hosono, *J. Appl. Phys.* **105**, 093916 (2009).
- ¹⁴ A. Pandey, R. S. Dhaka, J. Lamsal, Y. Lee, V. K. Anand, A. Kreyssig, T. W. Heitmann, R. J. McQueeney, A. I. Goldman, B. N. Harmon, A. Kaminski, and D. C. Johnston, *Phys. Rev. Lett.* **108**, 087005 (2012).
- ¹⁵ J.-X. Zhu, R. Yu, H. Wang, L. L. Zhao, M. D. Jones, J. Dai, E. Abrahams, E. Morosan, M. Fang, and Q. Si, *Phys. Rev. Lett.* **104**, 216405 (2010).
- ¹⁶ A. Georges, L. de’ Medici, and J. Mravlje, *Annual Review of Condensed Matter Physics* **4**, 137 (2013).
- ¹⁷ J. P. Perdew, K. Burke, and M. Ernzerhof, *Phys. Rev. Lett.* **77**, 3865 (1996).
- ¹⁸ P. Giannozzi, S. Baroni, N. Bonini, M. Calandra, R. Car, C. Cavazzoni, D. Ceresoli, G. L. Chiarotti, M. Cococcioni, I. Dabo, A. D. Corso, S. de Gironcoli, S. Fabris, G. Fratesi, R. Gebauer, U. Gerstmann, C. Gougoussis, A. Kokalj, M. Lazzeri, L. Martin-Samos, N. Marzari, F. Mauri, R. Mazzarello, S. Paolini, A. Pasquarello, L. Paulatto, C. Sbraccia, S. Scandolo, G. Sclauzero, A. P. Seitsonen, A. Smogunov, P. Umari, and R. M. Wentzcovitch, *Journal of Physics: Condensed Matter* **21**, 395502 (2009).
- ¹⁹ P. Blaha, K. Schwarz, G. Madsen, D. Kvasnicka, and J. Luitz, *WIEN2K: An Augmented Plane Wave + Local Orbitals Program for Calculating Crystal Properties* (Karlheinz Schwarz, Techn. Universität Wien, Austria, Wien, Austria, 2001).
- ²⁰ A. A. Mostofi, J. R. Yates, Y.-S. Lee, I. Souza, D. Vanderbilt, and N. Marzari, *Computer Physics Communications* **178**, 685 (2008).
- ²¹ C. Wang, M.-q. Tan, C.-m. Feng, Z.-f. Ma, S. Jiang, Z.-a. Xu, G.-h. Cao, K. Matsubayashi, and Y. Uwatoko, *Journal of the American Chemical Society* **132**, 7069 (2010).
- ²² T. Miyake, K. Nakamura, R. Arita, and M. Imada, *Journal of the Physical Society of Japan* **79**, 044705 (2010).
- ²³ L. de’ Medici, A. Georges, and S. Biermann, *Phys. Rev. B* **72**, 205124 (2005).
- ²⁴ A. Georges, G. Kotliar, W. Krauth, and M. J. Rozenberg, *Rev. Mod. Phys.* **68**, 13 (1996).
- ²⁵ M. Caffarel and W. Krauth, *Phys. Rev. Lett.* **72**, 1545 (1994).
- ²⁶ M. Capone, L. de’ Medici, and A. Georges, *Phys. Rev. B* **76**, 245116 (2007).
- ²⁷ M. Ferrero and O. Parcollet, “TRIQS - a toolbox for research on interacting quantum systems,” <https://arxiv.org/abs/1308.4013>.
- ²⁸ M. Aichhorn, L. Pourovskii, V. Vildosola, M. Ferrero, O. Parcollet, T. Miyake, A. Georges, and S. Biermann, *Phys. Rev. B* **80**, 085101 (2009).
- ²⁹ M. Aichhorn, L. Pourovskii, and A. Georges, *Phys. Rev. B* **84**, 054529 (2011).
- ³⁰ L. de’ Medici, S. R. Hassan, M. Capone, and X. Dai, *Phys. Rev. Lett.* **102**, 126401 (2009).
- ³¹ L. de’ Medici, “Weak and strong correlations in Iron pnictides” in *Iron-based superconductivity*, Springer Series in Materials Science, Vol. 211, Johnson, Peter D., Xu, Guangyong, Yin, Wei-Guo (Eds.), 2015.
- ³² R. B. Lehoucq, D. C. Sorensen, and C. Yang, “Arpack users guide,” (1997), (SIAM, Philadelphia).
- ³³ G. Giovannetti, M. Aichhorn, and M. Capone, *Phys. Rev. B* **90**, 245134 (2014).
- ³⁴ M. Greger, M. Sekania, and M. Kollar, [arxiv.org:1312.0100](https://arxiv.org/abs/1312.0100).